Astron. Astrophys. 99, 126–140 (1981)

ASTRONOMY
AND
ASTROPHYSICS

Tidal Evolution in Close Binary Systems

P. Hut

Astronomical Institute, University of Amsterdam, Roetersstraat 15, 1018 WB Amsterdam, The Netherlands

Received October 2, accepted December 16, 1980

Summary. The weak friction model for tidal interaction in a close binary system is investigated, in which the tides assume their equilibrium shape, but with a constant time lag (Darwin, 1879; Alexander, 1973). From this model differential equations are derived for the tidal evolution of several orbital and rotational parameters, using energy and angular momentum considerations only. The behaviour of the solutions to these equations is investigated.

First a local linear analysis is made of the approach towards a stable equilibrium configuration. Several time scales are introduced and compared, including a pseudo-synchronization time scale, which describes a near synchronization of revolution and rotation around periastron. Then a global analysis is presented for unrestricted eccentricity. A classification is made of all different types of tidal evolution behaviour, determined by only one parameter α, defined as the ratio of orbital to rotational angular momentum at the equilibrium configuration.

Increasing α above certain critical values qualitatively changes the global pattern of tidal evolution. A few examples are instability against circularity of the orbit, arising only for $\alpha > 10.932$, and instability against coplanarity of the orbital and equatorial planes, setting in above $\alpha > 21.532$. For several values of α the equations for tidal evolution are integrated numerically to illustrate the global flow pattern, as well as the details of the approach to an equilibrium configuration or a collision of the two stars.

Key words: binary stars – celestial mechanics – tidal evolution – X-ray binaries

1. Introduction

In a detached close binary, tidal evolution will continually change the orbital and rotational system parameters. Ultimately either an equilibrium state will be reached asymptotically, or the two stars will spiral in towards each other at an increasing rate, leading to a collision. An equilibrium state is characterized by coplanarity (the equatorial planes of the two stars coincide with the orbital planes), circularity (of the orbit) and corotation (the rotation periods of the stars equal the revolution period).

Such an equilibrium state is stable (unstable) if more (less) than three quarters of the total angular momentum are in the form of orbital angular momentum, as proved in a limited case by Counselman (1973) and more generally by Hut (1980).

The existence and stability properties of equilibrium states can be investigated by energy and angular momentum considerations alone. Tidal dissipation decreases the total orbital and rotational energy, while conserving the total angular momentum, allowing only an exchange between orbital and rotational angular momentum. However, in order to investigate the way in which an equilibrium state is approached, a specific model of tidal interaction must be given. Only then can we compare the time scales for changes in different orbital parameters such as eccentricity, semimajor axis, inclination and rotational velocity.

In the following a simple model will be used to derive explicit equations of tidal evolution for the parameters mentioned above. In this model the stars possess tides lagging by a constant small time with respect to their equilibrium value, as introduced first by Darwin (1879). Because of its mathematical simplicity many features can be computed exactly in this model. Also for more realistic models these features will still be of at least qualitative relevance, just as polytropes are often illustrative for problems in stellar structure.

In Sect. 2 an elementary derivation is given of the perturbing tidal forces in the model under consideration. In the first two appendices these perturbations are used to derive differential equations for the evolution of several orbital and rotational parameters of the binary system. Everywhere physical clarity is stressed, and energy and angular momentum considerations are used directly instead of the general perturbation techniques of celestial mechanics.

In Sect. 3 the tidal evolution equations are analysed locally around equilibrium configurations. Time scales are derived for the rate of change of the semimajor axis and the rotational velocity, approaching their equilibrium values, as well as for the eccentricity and inclination, which go to zero asymptotically. For the case where nearly all angular momentum is in the orbit a new concept of pseudo-synchronization is introduced.

In Sect. 4 the global aspects of the same tidal evolution equations are analyzed. Far from equilibrium many features are important which were completely overlooked in the local linear analysis around equilibrium. For the case of small inclination, but arbitrary eccentricity, a complete classification is made of all types of tidal evolution possible in the model under consideration. Some details of computations are given in Appendix C. Finally in Sect. 5 a discussion and conclusions are presented.

2. The Weak Friction Model for Tidal Interaction

Tidal interaction is an important factor in changing the orbit of a close detached binary. Each star raises tides on the surface of the other. Various dissipation mechanisms cause these tides to deviate from an instantaneous equipotential shape. This results in a

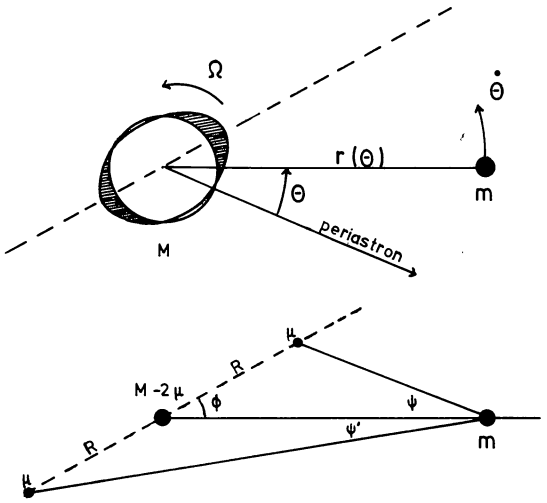

Fig. 1. Tides raised on the primary, with mass M, by the companion, with mass m, are approximated as point masses, with mass μ, to compute the perturbing tidal force reacting back on the companion. See text for definitions of symbols used

misalignment of the tides with respect to the line joining the centers of the two stars, which produces a torque component in the gravitational attraction of the stars. Via this spin-orbit coupling angular momentum is exchanged between the orbit and the rotation of each star. At the same time energy is dissipated in the tides, which diminishes the total energy of orbit and rotation. Even without a misalignment in the direction of the tides, energy will be dissipated if the amplitude of the tides lags in time with respect to equipotential surfaces, although no angular momentum is exchanged. In all cases the orbital parameters will change, and either asymptotically approach an equilibrium state, or lead to an accelerated spiralling in of the two stars (Counselman, 1973; Hut, 1980).

A detailed description of the evolution in time of the orbital elements caused by tidal effects cannot be given in a general form. One of the major complications arises from the possibility that the stars can be forced to oscillate in a variety of eigen modes. For an excellent review, the reader is referred to Zahn (1977).

In order to get a general qualitative picture of tidal evolution, one can investigate a simple model in which only equilibrium tides are described, with very small deviations in position and amplitude with respect to equipotential surfaces. Dynamical tides, where the stars oscillate, are then neglected. Choosing a mathematically simple description of the deviations from equilibrium makes it possible to discuss tidal evolution in a quantitative way. This can be compared with the use of polytropes in stellar evolution.

The weak friction model, which we will investigate, was discussed for the first time by Darwin (1879) and recently in detail by Alexander (1973). They assumed a constant time lag, where the tidally deformed surface of a star always assumes the equipotential surface it would have formed a constant time τ ago, in the absence of dissipation. As seen by an observer corotating with the surface of one star, the other star would raise a tidal bulge on his star misaligned by an angle proportional to the apparent angular velocity of the other star. As seen by a fixed observer, the tidal bulge would lag (or lead) with respect to the companion star if the rotational angular frequency Ω of the first star would be less (or greater) than the orbital angular velocity n. The case $\Omega > n$ is depicted in Fig. 1.

The motivation for this simple model of equilibrium tides stems partly from physical arguments (Zahn, 1977), but mainly from its mathematical simplicity. The model gives a good description of viscous dissipation (which seems however not to be relevant for tidal evolution in binary stars), and an approximate description of turbulent dissipation in convective envelopes (which is relevant for light main sequence stars). But in any case where equilibrium tides are more important than dynamical tides, we expect this model to be at least qualitatively correct, in that the misalignment angle (ϕ in Fig. 1) will be a monotonically increasing function of $\Omega - n$, the difference between rotational and orbital frequency. In the present model this function is approximated by a linear expression.

Other discussions of the weak friction model, and applications to binary stars and planet-satellite systems, are presented by Kopal (1978) and Mignard (1979, 1980), respectively, which include many additional references.

To simplify the discussion, one star (to be called the companion) is assumed to be point-like, so that only on the other star (the primary) tides will be raised. This gives already a realistic description of an X-ray binary or other binaries where the companion is a compact object; a white dwarf, neutron star or black hole. In the more general case the present analysis can be simply applied twice, switching the role of primary and companion and adding both effects, since only coupling between spin and orbit is important; spin-spin coupling is completely negligible.

The differential equations governing the rate of change of the orbital and rotational parameters are derived in an elegant and rather sophisticated way by Alexander (1973). Here a simple derivation will be given using energy and angular momentum considerations only, without using the whole machinery of celestial mechanics. Only the leading order (quadrupole) deviation of the surface of the primary will be treated, and therefore only leading powers in the small quantity R/r will be considered, where R is the radius of the primary and r the distance between the centers of both stars. In this approximation, the tides can be replaced by point masses at the surface of the primary with a mass μ each (see Fig. 1), where approximately

$$\mu = \frac{1}{2} km \left(\frac{R}{r}\right)^3 . \tag{1}$$

Here m is the mass of the companion and k the apsidal motion constant of the primary (Lecar et al., 1976). The factor m/r^3 follows from the tidal gravitational force, exerted by the companion, while the apsidal motion constant takes into account the structure of the primary, especially the central condensation (a higher value of which corresponds to a lower k; for realistic stars k has a value of ~ 0.1–0.01).

Without dissipation, μ would be given by (1), while the position angle ϕ would be $\phi = 0$ (Fig. 1); i.e. the tides would be aligned. In the present model, dissipation introduces a constant small time lag τ, such that both amplitude and direction of the tides are slightly changed. In the following, only terms linear in τ will be retained.

The amplitude lag gives

$$\mu(t) = \tfrac{1}{2} km R^3 \{r(t-\tau)\}^{-3} , \tag{2}$$

where $r(t-\tau)$ indicates the distance of the two stars at time $t-\tau$. To lowest order in τ

$$\mu(t) = \frac{1}{2} km \left(\frac{R}{r}\right)^3 \left(1 + 3\frac{\dot{r}}{r}\tau\right), \tag{3}$$

where $\dot{r}=dr/dt$. The lag in direction results in a position angle

$$\phi=(\Omega-\dot{\theta})\tau, \tag{4}$$

where Ω and $\dot{\theta}$ are the rotational and instantaneous orbital angular velocity, respectively (θ is the true anomaly).

Now we can compute the perturbed gravitational force between the two stars. As a simplification we start with the restriction that the orbit coincides with the equatorial plane of the primary. A finite value of the inclination will be taken into account later. From Fig. 1 we have

$$\begin{aligned}\boldsymbol{F}=\frac{Mm}{M+m}\ddot{\boldsymbol{r}}=&-G\frac{(M-2\mu)m}{r^2}\hat{r}\\&-G\frac{\mu m}{r^2+R^2-2rR\cos\phi}\{\cos\psi\hat{r}-\sin\psi\hat{\theta}\}\\&+G\frac{\mu m}{r^2+R^2+2rR\cos\phi}\{\cos\psi'\hat{r}-\sin\psi'\hat{\theta}\},\end{aligned} \tag{5}$$

where μ and ϕ are given by Eqs. (3) and (4); $\hat{r}$ and $\hat{\theta}$ are unit vectors in the r and θ direction and G is the gravitational constant. The angles ψ and ψ' as indicated in Fig. 1, are given by

$$\sin\psi=\frac{R\sin\phi}{(r^2+R^2-2rR\cos\phi)^{1/2}}, \tag{6}$$

$$\sin\psi'=\frac{R\sin\phi}{(r^2+R^2+2rR\cos\phi)^{1/2}}. \tag{7}$$

Expression (5) has to be developed to 5th order in R/r to find the leading contribution to the tidal perturbing force:

$$\boldsymbol{F}=-G\frac{Mm}{r^2}\left\{\hat{r}+3\frac{m}{M}\left(\frac{R}{r}\right)^5 k\left[\left(1+3\frac{\dot{r}}{r}\tau\right)\hat{r}-(\Omega-\dot{\theta})\tau\hat{\theta}\right]\right\}. \tag{8}$$

The first term is the Newtonian attraction between two point masses, while the other terms represent a perturbing acceleration, which causes a slow change of orbital parameters. We will be interested mainly in the semimajor axis a and the eccentricity e, together with the rotational angular velocity Ω.

The rates of change of a and e can be readily obtained by standard perturbation methods (see e.g. Brouwer and Clemence, 1961), after which the change in Ω follows from conservation of total angular momentum. However, in Appendix A a simple and physically more transparent derivation is given. First the torque resulting from the perturbing force is calculated, and its effects on the orbital elements a and e and on Ω. Secondly, the time delay in the amplitude of the tides is taken into account, which gives a comparable change in a and e (but not in Ω, since no angular momentum is transferred). The derivation, as presented in Appendix A, is similar to that given by Lecar et al. (1976) for the perturbing torque. However, these authors overlooked the amplitude delay effect, and therefore obtained different results.

The resulting tidal evolution equations are

$$\frac{da}{dt}=-6\frac{k}{T}q(1+q)\left(\frac{R}{a}\right)^8\frac{a}{(1-e^2)^{15/2}}\cdot\left\{f_1(e^2)-(1-e^2)^{3/2}f_2(e^2)\frac{\Omega}{n}\right\}, \tag{9}$$

$$\frac{de}{dt}=-27\frac{k}{T}q(1+q)\left(\frac{R}{a}\right)^8\frac{e}{(1-e^2)^{13/2}}\cdot\left\{f_3(e^2)-\frac{11}{18}(1-e^2)^{3/2}f_4(e^2)\frac{\Omega}{n}\right\}, \tag{10}$$

$$\frac{d\Omega}{dt}=3\frac{k}{T}\frac{q^2}{r_g^2}\left(\frac{R}{a}\right)^6\frac{n}{(1-e^2)^6}\cdot\left\{f_2(e^2)-(1-e^2)^{3/2}f_5(e^2)\frac{\Omega}{n}\right\}, \tag{11}$$

where

$$f_1(e^2)=1+\tfrac{31}{2}e^2+\tfrac{255}{8}e^4+\tfrac{185}{16}e^6+\tfrac{25}{64}e^8$$

$$f_2(e^2)=1+\tfrac{15}{2}e^2+\tfrac{45}{8}e^4+\tfrac{5}{16}e^6$$

$$f_3(e^2)=1+\tfrac{15}{4}e^2+\tfrac{15}{8}e^4+\tfrac{5}{64}e^6$$

$$f_4(e^2)=1+\tfrac{3}{2}e^2+\tfrac{1}{8}e^4$$

$$f_5(e^2)=1+3e^2+\tfrac{3}{8}e^4.$$

Here $n=G^{1/2}(M+m)^{1/2}a^{-3/2}$ is the mean orbital angular velocity and the radius of gyration r_g is defined as $I=M(r_gR)^2$, where I is the moment of inertia of the primary. Furthermore $q=\dfrac{m}{M}$ is the mass ratio of the two stars and

$$T=\frac{R^3}{GM\tau}=\frac{1}{4\pi^2}\left(\frac{P_s}{\tau}\right)P_s \tag{12}$$

is a typical time scale on which significant changes in the orbit take place through tidal evolution. P_s is the orbital period of a test particle moving in a grazing orbit over the surface of the primary; in units of P_s the tidal time scale T is the inverse of the tidal lag time.

Until now we have limited ourselves to the case of coplanarity. Deviations from coplanarity can be expressed in terms of the inclination i, the angle between the orbital plane and the equatorial plane of the primary. Other orbital elements, such as the longitude of the ascending node and the argument of periastron, are of no interest for the present discussion. They change rapidly due to rotational effects such as spin precession and apsidal motion, which are effective on much shorter time scales than tidal effects (Alexander, 1973).

In Appendix B the rate of change of i is computed to first order in i. There are two reasons for this restriction. First of all, X-ray binaries will generally start off after a supernova explosion with an appreciable eccentricity, possibly close to unity, because of the sudden mass loss to the system. But, if the initial binary system has been aligned ($i=0$), a finite inclination can only be achieved by an asymmetry in the supernova explosion, which is not expected to be very big. The other reason for treating the inclination only linearly is mathematical simplicity: to this accuracy no changes are necessary in Eqs. (9)–(11), which would otherwise involve cos$i$ factors. In Appendix B again physical clarity and simplicity are stressed. A more rigorous derivation and more complete results are given by Alexander (1973).

From Appendix B it follows that

$$\frac{di}{dt}=-3\frac{k}{T}\frac{q^2}{r_g^2}\left(\frac{R}{a}\right)^6(1-e^2)^{-6}\frac{n}{\Omega}i\cdot\left\{f_2(e^2)-\frac{1}{2}(1-\eta)\frac{\Omega}{n}(1-e^2)^{3/2}f_5(e^2)\right\}, \tag{13}$$

where $f_2(e^2)$ and $f_5(e^2)$ are the same expressions defined before in Eq. (11), and

$$\eta=\frac{I\Omega}{h}=r_g^2\frac{M+m}{m}\left(\frac{R}{a}\right)^2(1-e^2)^{-1/2}\frac{\Omega}{n} \tag{14}$$

is the ratio of the rotational and the orbital angular momentum.

The behaviour of the solutions to the four tidal evolution equations (9)–(11), and (13) will be analyzed in detail around equilibrium in Sect. 3, and far from equilibrium in Sect. 4. A few observations can be made readily for the simple case of near coplanarity ($i \simeq 0$) and near circularity ($e \simeq 0$), but arbitrary deviations from corotation ($\Omega \neq n$). All power series $f_i(e^2)$ are now approximately unity. As we would expect, for $\Omega > n$ angular momentum is transferred from spin to orbit, since Eqs. (9) and (11) show that $\dot{\Omega} < 0$ and $\dot{a} > 0$. Equation (10) marks the onset of instability of the circularity of the orbit at $\Omega = \frac{18}{11} n$: higher rotation rates give $\dot{e} > 0$. Finally Eq. (13) shows that instability against a growing inclination starts when the orbital period becomes slightly more than twice the rotation period, namely for $\Omega = 2n(1-\eta)^{-1}$. This factor of two, for small inclination, can easily be explained: for $\Omega > n$, the companion continually exerts a torque on the leading tidal bulges (Fig. 1), thereby diminishing the component $\Omega_{||}$ of $\boldsymbol{\Omega}$, parallel to the orbital angular momentum $\boldsymbol{h}$. At the same time $\Omega_{\perp}$, the component of $\boldsymbol{\Omega}$ perpendicular to $\boldsymbol{h}$, also decreases. This latter effect stems from tidal bulges lagging in latitude, with respect to an observer attached to the surface of the primary. But the sinusoidal movement in latitude of the tidal bulges produces an average transverse lag angle only half the value of the lag angle produced by a similar, but monotonous, movement in longitude. Thus the factor of two in Eq. (13) originates from the difference in effectivity of the periodic latitudinal and the monotonic longitudinal lag of the tidal bulges in the corotating frame.

3. Time Scales

Tidal interaction can lead either to a spiralling in of the two stars, followed by a collision, or to the evolution towards an equilibrium state, characterized by coplanarity ($i = 0$), circularity ($e = 0$) and corotation ($\Omega = n$). In the last case the parameters a, e, Ω, and i will asymptotically reach their equilibrium values, but on different time scales. Both the absolute and relative values of these time scales are of great observational importance. Knowledge of these quantities can give a general impression of the tidal evolution of observed binary systems. Moreover, in cases where only some of the parameters mentioned are observed, knowledge of tidal evolution time scales can give a reasonable impression of likely values for the unobserved parameters.

In this section, we will use the weak friction model introduced before to compare the time scales of alignment, circularization and synchronization. To investigate the asymptotic evolution towards equilibrium, we can linearize the Eqs. (9)–(11), and (13) around the equilibrium state. We can describe the deviations from equilibrium in dimensionless form by defining

$$x = \frac{a - a_0}{a_0} \tag{15}$$

and

$$y = \frac{\Omega - \Omega_0}{\Omega_0}, \tag{16}$$

where the equilibrium values a_0 and $\Omega_0 = n_0$ can be determined implicitly from the total angular momentum L with Eq. (A2):

$$L = I\Omega_0 + h = MR^2 r_g^2 \Omega_0 + G^{2/3}(M+m)^{-1/3} Mm \Omega_0^{-1/3}, \tag{17}$$

according to Kepler's third law. Denoting linearized approximations of x, e, y, i by $\bar{x}, \bar{e}, \bar{y}, \bar{i}$, the linearized equations read

$$\frac{d\bar{x}}{dt} = 3\frac{k}{T} q(1+q)\left(\frac{R}{a_0}\right)^8 \{3\bar{x} + 2\bar{y}\}, \tag{18}$$

$$\frac{d\bar{e}}{dt} = -\frac{21}{2}\frac{k}{T} q(1+q)\left(\frac{R}{a_0}\right)^8 \bar{e}, \tag{19}$$

$$\frac{d\bar{y}}{dt} = -\frac{3}{2}\frac{k}{T}\frac{q^2}{r_g^2}\left(\frac{R}{a_0}\right)^6 \{3\bar{x} + 2\bar{y}\}, \tag{20}$$

$$\frac{d\bar{i}}{dt} = -\frac{3}{2}\frac{k}{T}\frac{q^2}{r_g^2}\left(\frac{R}{a_0}\right)^6 (1+\eta)\bar{i}. \tag{21}$$

These expressions can be simplified considerably by defining the dimensionless quantity

$$\alpha = \frac{h_0}{I\Omega_0} = \frac{q}{1+q}\frac{1}{r_g^2}\left(\frac{a_0}{R}\right)^2, \tag{22}$$

the ratio of orbital and rotational angular momentum at the (unique) stable equilibrium configuration (i.e. $\alpha = \eta_0^{-1}$). Remember that an equilibrium state is stable if and only if $\alpha > 3$ (Counselman, 1973; Hut, 1980). Introducing a "slow" time

$$t' = kq(1+q)\left(\frac{R}{a_0}\right)^8 \frac{t}{T}, \tag{23}$$

the linearized equations read

$$\frac{d\bar{x}}{dt'} = 3(3\bar{x} + 2\bar{y}), \tag{24}$$

$$\frac{d\bar{e}}{dt'} = -\frac{21}{2}\bar{e}, \tag{25}$$

$$\frac{d\bar{y}}{dt'} = -\frac{3}{2}\alpha(3\bar{x} + 2\bar{y}), \tag{26}$$

$$\frac{d\bar{i}}{dt'} = -\frac{3}{2}(1+\alpha)\bar{i}. \tag{27}$$

The Eqs. (24) and (26) are dependent since angular momentum is conserved during tidal evolution. The total angular momentum L is given by

$$L = I\Omega + h = MR^2 r_g^2 \Omega + G^{1/2} Mm(M+m)^{-1/2} a^{1/2}(1-e)^{1/2}. \tag{28}$$

Using Kepler's third law

$$\Omega_0 = n_0 = G^{1/2}(M+m)^{1/2} a_0^{-3/2}, \tag{29}$$

the previous expression reads

$$L = MR^2 r_g^2 \Omega_0 \left\{\frac{\Omega}{\Omega_0} + \alpha\left(\frac{a}{a_0}\right)^{1/2}(1-e^2)^{1/2}\right\}, \tag{30}$$

or in a linearized version

$$\bar{L} = MR^2 r_g^2 \Omega_0 \{1 + \bar{y} + \alpha(1 + \tfrac{1}{2}\bar{x})\}. \tag{31}$$

Constancy of L thus gives

$$\bar{y} = -\frac{\alpha}{2}\bar{x} \tag{32}$$

which immediately explains the relation between (24) and (26).

The solutions of Eqs. (24)–(27) are simply

$$\bar{x}(t')=\bar{x}(0)e^{-t'/t_{\bar{x}}}, \quad \text{etc.}$$

with time scales

$$t_{\bar{x}}=t_{\bar{y}}=\frac{1}{3(\alpha-3)},$$

$$t_{\bar{e}}=\frac{2}{21}, \tag{33}$$

$$t_{\bar{i}}=\frac{2}{3(\alpha+1)}.$$

To interprete these results, we have to distinguish between three cases:

(i) $\alpha>3$, but $\alpha-3\ll 1$. This corresponds to a binary system where the equilibrium state is just marginally stable, the rotational angular momentum being only slightly less than a quarter of the total angular momentum. Here $t_{\bar{x}}=t_{\bar{y}}\gg t_{\bar{e}}\approx t_{\bar{i}}$. The eccentricity and inclination will tend to zero relatively quickly, but synchronization (and adjustment of the semimajor axis) takes much more time.

(ii) α of order 7, i.e. $4\lesssim\alpha\lesssim 10$. The equilibrium state is further away from instability, but the rotational angular momentum is still comparable in magnitude with the orbital angular momentum. This means that the companion star is either much lighter than the primary, or orbits very close to its surface. In this case we have $t_{\bar{x}}=t_{\bar{y}}\approx t_{\bar{e}}\approx t_{\bar{i}}$. All parameters change roughly at the same pace.

(iii) $\alpha\gg 7$. The orbital angular momentum is much larger than the rotational angular momentum. This can be the case when the companion is the most massive star, or when the separation between the stars is fairly large. Here $t_{\bar{e}}\gg t_{\bar{i}}\approx t_{\bar{x}}=t_{\bar{y}}$. The inclination decreases relatively quickly, while at the same time rotation tends to synchronise with revolution. The eccentricity of the orbit diminishes much slower. There is one problem in the last case: It looks as if the rotational period quickly settles to the equilibrium orbital period to achieve synchronization, but this is deceiving. Since the eccentricity changes relatively slowly, the orbit will remain rather eccentric for a long time. During each orbit the tidal interaction will then be most important around periastron. This can be seen from the strong distance dependence of the tidal force in Eq. (8): $F\sim r^{-7}$. It is to be expected that the rotation of the primary quickly synchronizes with the instantaneous orbital angular velocity at periastron. This pseudo-synchronization therefore keeps the rotational period shorter than the orbital period as long as the eccentricity stays finite.

An interesting example in another context is the pseudo-synchronization of Mercury, where three rotations take place during two revolutions, but rotational and orbital angular velocity are comparable around periastron (Fig. 2). In this case, however, the rotation and revolution are locked in in a 3:2 resonance since Mercury, being a solid body, has a permanent asymmetry in its shape. In a binary the stars, being gaseous bodies, have no built-in asymmetry. Therefore tidal evolution continues until the orbit becomes circular and real synchronization will be achieved.

This can be made more quantitative if we repeat the linear analysis using the same variables, but taking e^2 instead of e as the eccentricity parameter. This is a natural choice since e occurs only quadratic in Eqs. (9), (11), and (13), and also in Eq. (10) after writing de^2/dt. Especially for case (iii), $\alpha\gg 7$, this is also a reasonable choice, since t_e is much larger than the other time scales.

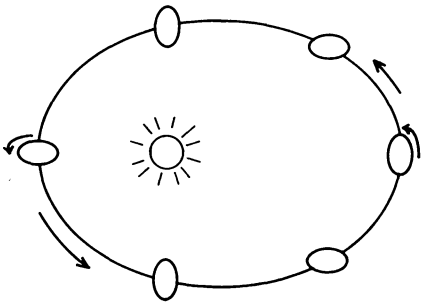

Fig. 2. The 2:3 resonance of orbit and rotation of Mercury. Through a permanent asymmetry in its shape, exaggerated here, Mercury is locked in a state of pseudo-synchronization of orbit and rotation around perihelium

Instead of (24)–(27) we now have

$$\frac{d}{dt'}\begin{pmatrix}\tilde{x}\\ \tilde{e}^2\\ \tilde{y}\\ \tilde{i}\end{pmatrix}=\frac{3}{2}\begin{pmatrix}6 & -38 & 4 & 0\\ 0 & -14 & 0 & 0\\ -3\alpha & 12\alpha & -2\alpha & 0\\ 0 & 0 & 0 & -(1+\alpha)\end{pmatrix}\begin{pmatrix}\tilde{x}\\ \tilde{e}^2\\ \tilde{y}\\ \tilde{i}\end{pmatrix}, \tag{34}$$

where $\tilde{e}^2$ etc. now indicates linearization with respect to e^2, instead of e.

Again these equations are not independent, since the determinant of the matrix in Eq. (34) vanishes. As shown before, this follows from angular momentum conservation, since Eq. (30) now linearizes to

$$\tilde{L}=MR^2r_g^2\Omega_0\{1+\tilde{y}+\alpha(1+\tfrac{1}{2}\tilde{x}-\tfrac{1}{2}\tilde{e}^2)\}. \tag{35}$$

Thus $\tilde{L}$ conservation gives

$$\tilde{y}=\frac{\alpha}{2}(-\tilde{x}+\tilde{e}^2),$$

consistent with Eq. (34).

The solution of Eq. (34), for $\alpha\neq 10$, is given by

$$\tilde{e}^2(t')=\tilde{e}^2(0)e^{-21t'}, \tag{36}$$

$$\tilde{i}(t')=\tilde{i}(0)e^{-\frac{3}{2}(1+\alpha)t'}, \tag{37}$$

$$\tilde{x}(t')=\left\{\tilde{x}(0)-\frac{\alpha-19}{\alpha-10}\tilde{e}^2(0)\right\}e^{-3(\alpha-3)t'}+\frac{\alpha-19}{\alpha-10}\tilde{e}^2(0)e^{-21t'}, \tag{38}$$

$$\tilde{y}(t')=\left\{\tilde{y}(0)-\frac{9\alpha}{2(\alpha-10)}\tilde{e}^2(0)\right\}e^{-3(\alpha-3)t'}+\frac{9\alpha}{2(\alpha-10)}\tilde{e}^2(0)^{-21t'}. \tag{39}$$

For the case that the two eigenvalues of the matrix of coefficients in Eq. (34) are degenerate, i.e. for $\alpha=10$, the solutions (38) and (39) have to be replaced by

$$\tilde{x}(t')=\{\tilde{x}(0)-27e^2(0)t'\}e^{-21t'}, \tag{40}$$

$$\tilde{y}(t')=\{\tilde{y}(0)+\tfrac{27}{2}\alpha e^2(0)t'\}e^{-21t'}. \tag{41}$$

Now we can read off the anticipated result: for $\alpha>10$, the first terms in Eqs. (38) and (39) decrease faster than the second terms. Thus the binary system approaches pseudo-synchronization, gov-

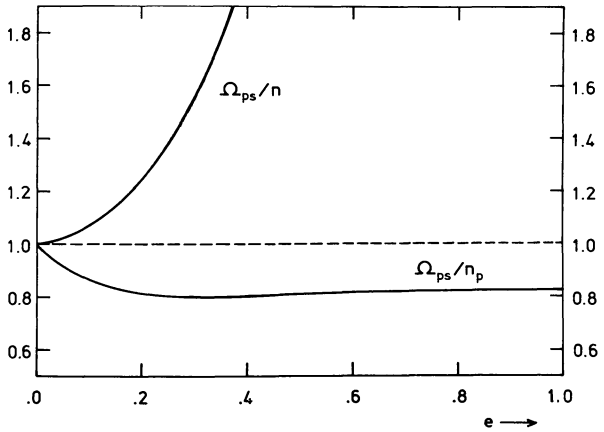

Fig. 3. The rotational angular velocity Ω_{ps} for pseudo-synchronization, expressed in units of the mean motion n, and of the orbital angular velocity at periastron n_p, as a function of eccentricity e

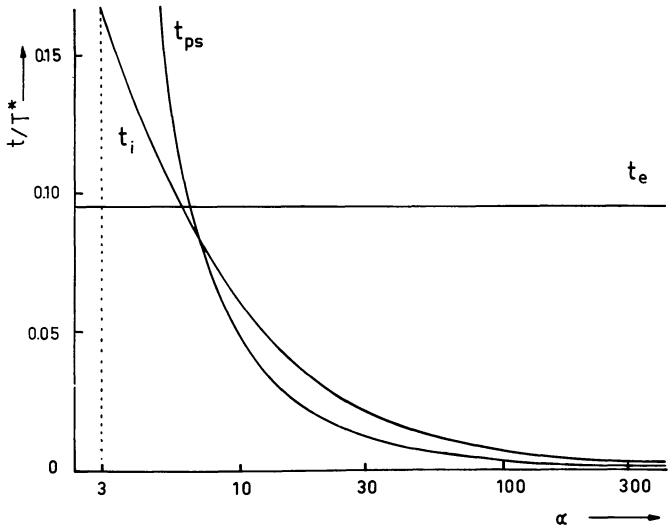

Fig. 4. Time scales for the approach of circularization t_e; of coplanarity t_i; and of pseudo-synchronization t_{ps}, expressed in units of a typical tidal time scale T^*, defined in Eq. (49)

erned by the second terms in Eqs. (38) and (39), independent of the initial values $\tilde{x}(0)$ and $\tilde{y}(0)$. As expected, pseudo-synchronization gives a higher rotational velocity than the equilibrium state: $y>0$ for large t' values in Eq. (39), which means $\Omega>\Omega_0$.

To be even more quantitative, we can go back to the original Eq. (11) for the rotational velocity. Pseudo-synchronization can be defined as $\Omega=\Omega_{ps}$ if $\dot{\Omega}=0$, i.e.:

$$\frac{\Omega_{ps}}{n}=\frac{1+\frac{15}{2}e^2+\frac{45}{8}e^4+\frac{5}{16}e^6}{(1+3e^2+\frac{3}{8}e^4)(1-e^2)^{3/2}} \tag{42}$$

or

$$\frac{\Omega_{ps}}{n}=1+6e^2+\frac{3}{8}e^4+\frac{223}{8}e^6+O(e^8). \tag{43}$$

Again it is clear that $\Omega\to n$ ($e\to 0$) while $\Omega>n$ ($e>0$).

Pseudo-synchronization is caused by the fact that tidal interaction is strongest around periastron. This can be seen most directly by comparing Ω_{ps} with $n_p=\dot{\theta}$ ($\theta=0$), the orbital angular velocity at periastron, which is given by

$$n_p=\frac{(1+e)^2}{(1-e^2)^{3/2}}n \tag{44}$$

[this follows immediately from Eqs. (A5) and (A8)]. Instead of Eq. (42) we can write

$$\frac{\Omega_{ps}}{n_p}=\frac{1+\frac{15}{2}e^2+\frac{45}{8}e^4+\frac{5}{16}e^6}{(1+3e^2+\frac{3}{8}e^4)(1+e)^2}. \tag{45}$$

For small eccentricity this can be expanded as

$$\frac{\Omega_{ps}}{n_p}=1-2e+\frac{15}{2}e^2-13e^3+\frac{41}{4}e^4+O(e^5), \tag{46}$$

while for large eccentricities

$$\frac{\Omega_{ps}}{n_p}\to\frac{33}{40}=0.825 \quad (e\to 1). \tag{47}$$

For all eccentricities

$$1>\frac{\Omega_{ps}}{n}>0.799, \tag{48}$$

where the minimum value occurs around $e=0.308$.

In Fig. 3, $\Omega_{ps}(e)$ is plotted twice, in units of n and n_p. At small eccentricity ($e\ll 0.2$), tidal interaction is important over the whole orbit, and $\Omega_{ps}\simeq n$ is a much better approximation than $\Omega_{ps}\simeq n_p$. For fairly large eccentricities ($e>0.2$), tidal interaction is only effective around periastron. A weighted average of the orbital angular velocity $\dot{\theta}$ around periastron is always slightly smaller than $\dot{\theta}_{\max}=n_p$, and therefore $\Omega_{ps}\lesssim n_p$.

Turning back to the original time scales, derived in Eq. (33), we now see their meaning: $t_{\bar{e}}$ and $t_{\bar{i}}$ are the time scales on which the eccentricity and inclination decrease exponentially. They are expressed in units of a "slow" time t', defined in Eq. (23), which correspond with a unit T^* of real time, where

$$T^*=\{kq(1+q)\}^{-1}\left(\frac{a_0}{R}\right)^8 T, \tag{49}$$

or using Eq. (12)

$$T^*=(4\pi^2kq)^{-1}\left(\frac{a_0}{R}\right)^8\frac{P_0}{\tau}P_0, \tag{50}$$

where P_0 is the orbital period of the equilibrium state. The time scale $t_{\bar{x}}=t_{\bar{y}}$ is really a pseudo-synchronization time scale t_{ps}. For small values of α, or a relatively large rotational angular momentum, t_{ps} is the time scale for synchronization, since circularization is achieved relatively quickly. For greater values of α, or a relatively large orbital angular momentum, t_{ps} indicates how much time it takes to synchronize a binary system around periastron in an eccentric orbit.

To summarize: the pseudo-synchronization time scale, or periastron synchronization time scale, is

$$t_{ps}=\frac{1}{3(\alpha-3)}T^*; \tag{51}$$

the time scale for circularization is

$$t_e=\tfrac{2}{21}T^*; \tag{52}$$

and the time scale for alignment is

$$t_i=\frac{2}{3(\alpha+1)}T^*. \tag{53}$$

These timescales are depicted in Fig. 4, as a function of α. Note that $\alpha > 3$ is required in order to guarantee the existence of an equilibrium state of the binary. It is easy to physically understand why $t_e \gg t_{ps} \simeq t_i$ for large values of α: synchronization and alignment both involve the rotation of the primary in an essential way. But circularization involves a property of the orbit only: even after the rotation is optimally adjusted through pseudo-synchronization, the orbit can stay rather eccentric for a long time. Only if the primary has an appreciable moment of inertia ($\alpha \lesssim 10$) rotational adaptation takes about as much time as orbital circularization.

4. Tidal Evolution Far from Equilibrium

In the previous section the asymptotic tidal evolution of a binary towards an equilibrium state is discussed. Time scales for the exponential relaxation of several parameters were found in a local analysis of the differential Eqs. (9)–(11), and (13) around equilibrium. Now we proceed to investigate the global structure of the solutions to these equations. To simplify the discussion, we will start with the restriction of coplanarity, i.e. $i=0$. Later we will discuss small inclination, again treated linearly.

In this case we are left with the three differential Eqs. (9)–(11), of which only two are independent since the total angular momentum L is conserved. Choosing as independent parameters the orbital elements a and e, we have to express Ω as a function of a, e and L:

$$\mathrm{L} = \mathrm{I}\Omega + \mathrm{h} = \mathrm{MR}^2 \mathrm{r}_g^2 \Omega + \mathrm{G}^{1/2}(\mathrm{M}+\mathrm{m})^{-1/2}\mathrm{Mma}^{1/2}(1-\mathrm{e}^2)^{1/2}, \quad (54)$$

where h is the orbital angular momentum, given by Eq. (A2) and I is the moment of inertia, given by Eq. (A26).

It is very convenient to introduce again the ratio α of the orbital and the rotational angular momentum of the binary at equilibrium:

$$\alpha = \frac{q}{1+q}\frac{1}{r_g^2}\left(\frac{a_0}{R}\right)^2, \quad (55)$$

where a_0 is the value of the semimajor axis in the equilibrium state. Note that α is a constant, independent of a and e, related to L and the other constants by

$$L = MR^2 r_g^2 \Omega_0 (1+\alpha), \quad (56)$$

where Ω_0 is the value of Ω at equilibrium. With Eq. (55) and Kepler's third law this can be written

$$L = G^{1/2} M m^{3/4} (M+m)^{-1/4} R^{1/2} r_g^{1/2} \alpha^{-3/4} (1+\alpha). \quad (57)$$

For applications to a specific binary system, this equation defines α implicitly in terms of observable parameters. Note that there are only solutions for $L \geqq L_{cr}$, where

$$L_{cr} = 4.3^{-3/4} G^{1/2} M m^{3/4} (M+m)^{-1/4} R^{1/2} r_g^{1/2}. \quad (58)$$

For $L > L_{cr}$, Eq. (55) admits two solutions α_+, α_- with $\alpha_+ > \alpha_-$; α_- corresponds with the unstable equilibrium state, and α_+ with the stable equilibrium. For a general analysis, see Hut (1980). Here we are only interested in α_+ which will simply be denoted by α.

We want to substitute Ω from Eq. (54) into the differential Eqs. (9) and (10) for a and e. Only the ratio Ω/n occurs, and from Eqs. (54), (55), and (57), again with Kepler's third law, the following surprisingly simple relation can be obtained:

$$\frac{\Omega}{n} = (1+\alpha)\tilde{a}^{3/2} - \alpha\tilde{a}^2(1-e^2)^{1/2}. \quad (59)$$

Here $\tilde{a}$ is a dimensionless quantity which expresses the semimajor axis in equilibrium units:

$$\tilde{a} = a/a_0. \quad (60)$$

The equations describing the evolution of a and e now read, using Eq. (10), (11), and (59), and the "slow" time t', defined in Eq. (23):

$$\frac{d\tilde{a}}{dt'} = -6\tilde{a}^{-7}(1-e^2)^{-15/2} \cdot \{g_1(e^2) + \alpha g_2(e^2)\tilde{a}^2 - (1+\alpha)g_3(e^2)(1-e^2)^{1/2}\tilde{a}^{3/2}\}, \quad (61)$$

$$\frac{de}{dt'} = -27\tilde{a}^{-8}(1-e^2)^{-13/2} \cdot \{g_4(e^2) + \frac{11}{18}\alpha g_5(e^2)\tilde{a}^2 - \frac{11}{18}(1+\alpha)g_6(e^2)(1-e^2)^{1/2}\tilde{a}^{3/2}\}, \quad (62)$$

where

$$g_1(e^2) = 1 + \tfrac{31}{2}e^2 + \tfrac{255}{8}e^4 + \tfrac{185}{16}e^6 + \tfrac{25}{64}e^8$$
$$g_2(e^2) = 1 + \tfrac{11}{2}e^2 - \tfrac{67}{8}e^4 - \tfrac{55}{16}e^6 + 5e^8 + \tfrac{5}{16}e^{10}$$
$$g_3(e^2) = 1 + \tfrac{13}{2}e^2 - \tfrac{15}{8}e^4 - \tfrac{85}{16}e^6 - \tfrac{5}{16}e^8$$
$$g_4(e^2) = 1 + \tfrac{15}{4}e^2 + \tfrac{15}{8}e^4 + \tfrac{5}{64}e^6$$
$$g_5(e^2) = 1 - \tfrac{1}{2}e^2 - \tfrac{15}{8}e^4 + \tfrac{5}{4}e^6 + \tfrac{1}{8}e^8$$
$$g_6(e^2) = 1 + \tfrac{1}{2}e^2 - \tfrac{11}{8}e^4 - \tfrac{1}{8}e^6.$$

Except for a proliferation of numerical coefficients, these two equations are remarkably simple. The only external parameter of this coupled system of differential equations is α, which characterizes the stable equilibrium state. The only dependence on M, m, R, and r_g comes in via the definitions of α and t', and the pattern of the flow in $(\tilde{a}, e)$-space, determined by $d\tilde{a}/de$, is completely fixed by a choice for α.

A few typical solutions to Eqs. (61) and (62) are plotted in $(\tilde{a}, e)$-diagrams (Figs. 5–8) for the cases $\alpha = 4$, 10, 25, and 100. In each case the two equilibrium configurations are indicated; a stable equilibrium at $(\tilde{a}_+, e) = (1, 0)$ and an unstable one at $(\tilde{a}_-, 0)$, where $\tilde{a}_-$ is the smallest of the two roots to the equation

$$\alpha\tilde{a}^2 - (1+\alpha)\tilde{a}^{3/2} + 1 = 0. \quad (63)$$

This follows directly from Eq. (59), for the case of corotation. For large α, $\tilde{a}_-$ can be approximated by

$$\tilde{a}_- = \alpha^{-2/3}(1 + \tfrac{2}{3}\alpha^{-1/3} + O(\alpha^{-1})). \quad (64)$$

It is clear from the linear analysis in Sect. 3, that $(1, 0)$ is a stable node, while $(\tilde{a}_-, 0)$ is a saddlepoint. This result is general, independent of the model of tidal interaction (Hut, 1980). Here it follows from Eq. (33): for $\alpha > 3$ all time scales are positive, making $(1, 0)$ an attractor. For $\alpha < 3$, $t_{\bar{e}}$ and $t_{\bar{i}}$ are positive, but $t_{\bar{x}} = t_{\bar{y}}$ is negative and therefore $(\tilde{a}_-, 0)$ is a saddlepoint. This can be seen also in Figs. 5–8, where the broken line indicates the separatrix. This flow line, ending at the unstable equilibrium, separates the $(\tilde{a}, e)$-plane into two sets of initial conditions. Tidal evolution starting in the upper left half of the plane ends at the stable equilibrium, while evolution in the lower right leads to a collision of the two stars ($\tilde{a} \to 0$).

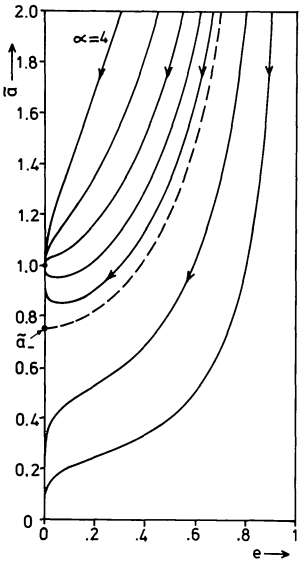

Fig. 5

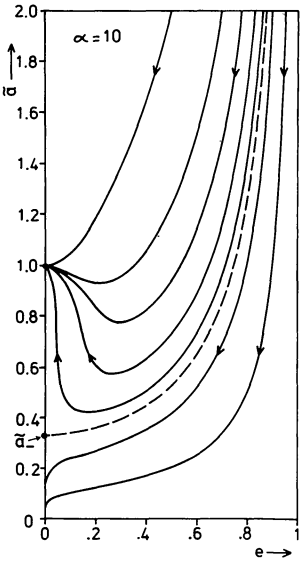

Fig. 6

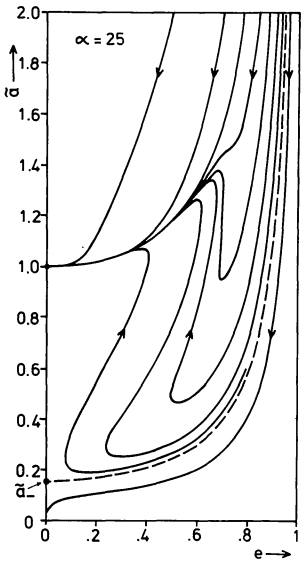

Fig. 7

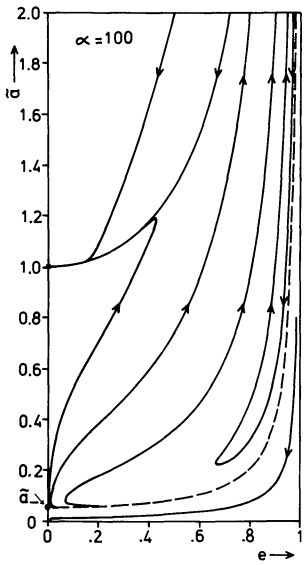

Fig. 8

Fig. 5–8. Flow lines of the solutions to the tidal evolution equations (61) and (62) for different values of α. The coordinates are e, the eccentricity, and $\tilde{a}$, the semimajor axis in units of its stable equilibrium value. Thus $\tilde{a}_+$ is unity and $\tilde{a}_-$, the value of $\tilde{a}$ at the unstable equilibrium, is defined implicitly in Eq. (63). The broken line is the flow line ending at the unstable equilibrium, separating the solutions ending in collision from the solutions ending at the stable equilibrium configuration

The qualitative form of the flow lines near equilibrium can be understood from the linear analysis leading to Eqs. (36)–(39). For $\alpha=4$, it follows from Eq. (33) that $t_{\tilde{x}}=t_{\tilde{y}}\gg t_e$ (see also Fig. 4), and the system tends to circularity much faster than to synchronization.

This can be seen in Fig. 5, where $e\to 0$ quickly before $\tilde{a}\to 1$. For $\alpha\geqq 10$, t_e is the largest timescale, and the binary system tends to pseudo-synchronization before circularization is completed. Thus the tidal evolution tracks in Figs. 6–8 approach each other at finite eccentricity before reaching the end point at equilibrium. For $\alpha<19$ the pseudo-synchronization track approaches the stable equilibrium from below ($\tilde{a}<1$). This follows from the negativity of the last term in the right hand sides of Eqs. (38) and (39) for large t', and can be seen in Fig. 6. For $\alpha>19$ stable equilibrium is generally approached from above ($\tilde{a}>1$), as is clear from Eq. (38) and Figs. 7 and 8.

For higher α values, the pattern of the evolutionary tracks is rather complicated. Unstable evolution always has decreasing $\tilde{a}$ and e, but flow lines ending at the stable equilibrium can turn around several times if the initial eccentricity at high $\tilde{a}$ is sufficiently high (Figs. 7 and 8). This phenomenon can be explained as follows.

Let us start with a system where $\alpha=25$ and the initial value of the semimajor axis is twice the equilibrium value ($\tilde{a}=2$) and the eccentricity is high, say $e=0.9$. This implies a rather close periastron passage, where most of the tidal interaction takes place. At high e, the orbital velocity is relatively rather high at periastron, and consequently the primary will be spun up: angular momentum is transferred from orbit to rotation, and both $\tilde{a}$ and e decrease. The orbit continues to shrink far under the stable equilibrium value ($\tilde{a}<1$), before the rotation of the primary has caught up with the orbital motion at periastron. Hereafter the orbit continues to circularize, which causes the orbital angular velocity at periastron to continue to decrease even at a stationary semimajor axis.

Consequently the rotation of the primary is now too fast, and the primary starts to spin down: angular momentum is transferred back again from spin to orbit. The orbit widens, and $\tilde{a}$ grows. At first e keeps diminishing, but if the difference in rotational and orbital motion at periastron becomes too large the eccentricity increases again. What happens is the inverse of the drag effect of the earth atmosphere on a satellite: the fast spinning primary accelerates the companion mainly around periastron. An example of this stage of evolution is the earth – moon system, where the rotation of the earth is slowed down and both the eccentricity and the semimajor axis of the lunar orbit increase through tidal interaction.

For a given semimajor axis the orbital angular momentum decreases with increasing eccentricity. Thus at $\tilde{a}=1$ and $e>0$ the orbit still has too little angular momentum and the primary still spins too rapidly. For the second time the binary system passes the equilibrium value $\tilde{a}=1$, this time overshooting to an orbit which is too wide again. The orbit stops growing around the time when pseudo-synchronization is achieved, where rotation and orbital motion are synchronized around periastron. Hereafter the orbit slowly settles to equilibrium, with decreasing $\tilde{a}$ and e. The reason is that the time scale t_e for circularization is much larger than the time scale t_{ps} for pseudo-synchronization for $\alpha\gg 7$ (see Fig. 4), as derived in Sect. 3. This effect can clearly be seen in Figs. 7 and 8, where neighbouring flow lines clutter around the pseudo-synchronization track before ending at the stable equilibrium point.

To summarize: at low values of α tidal evolution is rather simple, with eccentricity always decreasing. At higher α values, $\alpha\gg 7$, the rotational moment of inertia is relatively small. The binary system can go through stages of upspinning and down spinning before settling to pseudo-synchronization. Thereafter the eccentricity monotonically decreases to zero.

The global evolutionary behaviour discussed above can be illustrated more quantitatively as follows. From Eq. (61) we can

find all $(\tilde{a}, e)$-values for which $\tilde{a}$ is stationary by setting the expression within brackets equal to zero. In this way we can find all turning points for the evolution of the width of the orbit. In the same way we can determine the stationary points of the eccentricity from (62). As an example, the case $\alpha=25$ is depicted in Fig. 9: there is one curve on which $d\tilde{a}/dt'=0$, and one curve on which $de/dt'=0$. They devide the $(\tilde{a}, e)$-plane in three regions: in the outside region both $\tilde{a}$ and e decrease; in the region in between the two curves $\tilde{a}$ increases but e still decreases; and in the innermost region both $\tilde{a}$ and e increase.

In Fig. 9 are also indicated two parts of the curve on which the rotational angular velocity Ω is stationary, and thus pseudo-synchronization is achieved. This curve is obtained from Eq. (11) by putting the right hand side equal to zero, and using Eq. (59). In between the two parts of the curve Ω decreases while outside Ω increases. In the following analysis we will find that these two parts meet outside the figure to make one curve similar to those for $\tilde{a}$ and e, at least for the value $\alpha=25$. The dotted line indicates where $\Omega=0$, to the left of which the rotation is retrograde ($\Omega<0$).

Finally the stationary points of the inclination i can be found from Eq. (13). As is indicated in Fig. 9, these points also form one curve for $\alpha=25$. In the outer region the inclination decreases, while it increases in the inner region. Thus the assumption of zero inclination, made in the beginning of this section is only strictly consistent in the major part of the $(\tilde{a}, e)$-plane, outside the stationary inclination curve.

It is interesting to analyse the occurrence of the global features described above. Here only the results will be given; some details of the straightforward, but rather tedious analysis are given in Appendix C. The stationary curves in the $(\tilde{a}, e)$-plane for $\tilde{a}$, e, Ω and i occur as follows:

$\tilde{a}$ has a stationary curve for all $\alpha>3$. There is a critical value $\alpha\simeq 35.447$ so that for lower α values the curve looks qualitatively like the one in Fig. 9: there is an inner region, covering only a restricted eccentricity range, where $d\tilde{a}/dt'>0$; outside of this region $\tilde{a}$ decreases. For α bigger than the critical value the inner region reaches all the way to $e=1$, but approaches $e=1$ only at $\tilde{a}\to\infty$. Thus for $\alpha>35.447$ the $(\tilde{a}, e)$-plane is divided in three regions by two curves of stationary $\tilde{a}$.

e has no stationary curves for small α, in which case $de/dt'<0$ everywhere (see Figs. 5 and 6). Only for $\alpha\gtrsim 10.932$ a stationary curve exists, with an inner region in which e increases. This curve grows with increasing α, but always stays inside the curve where $\tilde{a}$ is stationary. Thus e can only increase if $\tilde{a}$ increases too. The stationary e curve meets the line $e=1$ at $\tilde{a}\to\infty$ at the same critical value $\alpha\simeq 35.447$ as the $\tilde{a}$ curve does.

Ω behaves qualitatively as $\tilde{a}$: for all $\alpha>3$ a stationary curve exists. In the inner region the primary spins down ($d\Omega/dt'<0$), while outside it spins up. This single curve again splits into two curves joining $e=1$ at infinity, but for a lower critical value $\alpha\simeq 27.062$. Thus we know that the two parts of the curve for stationary Ω, drawn in Fig. 9, meet at $e<1$, since $\alpha=25$ is smaller than this critical value.

i behaves at first qualitatively like e: no stationary curves exist for low α values, for which the inclination decreases everywhere. For $\alpha\gtrsim 21.532$ a single curve of stationary inclination forms, always inside the curve of stationary eccentricity. Thus the inclination can grow only if at the same time also the eccentricity and the semimajor axis grow. However, the inner region of growing inclination never reaches $e=1$: the curve of stationary inclination asymptotically reaches $e\simeq 0.9025$ for $\alpha\to\infty$. Thus for higher eccentricities the inclination always decreases.

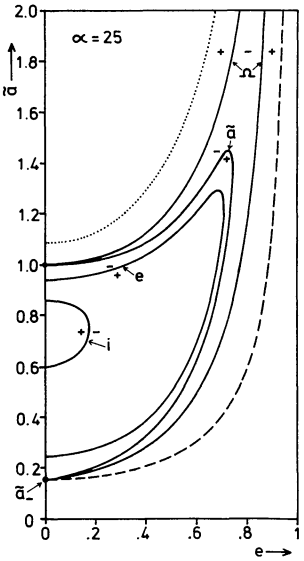

Fig. 9. Regions of different types of tidal evolution for $\alpha=25$. The broken line is the same as in Fig. 7 and the dotted line separates the upper region, where $\Omega<0$, from the lower region where $\Omega>0$

This concludes the survey of the main global features of tidal evolution according to the simple model of constant time lag in equilibrium tides. The most surprising result is the existence of so many critical α values where new global features appear, which went completely unnoticed in the linear analysis of the previous section. All five distinct possibilities are summarized in Table 1.

From the present discussion it is not yet clear how the binary system behaves for $e\to 1$, since $\tilde{a}\to\infty$ simultaneously. To investigate the high eccentricity limit, the tidal evolution equations have to be transformed to another system of more suitable coordinates, e.g., the periastron distance instead of the semimajor axis. This will be treated in a separate publication, where it will be shown that for $\alpha>35.447$ disruption of the binary system into a hyperbolic orbit is possible.

5. Discussion and Conclusions

Starting with the mathematically simple assumption of constant time lag for the equilibrium tides, perturbing tidal forces were derived. By averaging the effects of these perturbing forces over one orbit equations governing tidal evolution were found. The derivation, presented in Sect. 2 and in Appendices A and B, was kept elementary while stressing the physical principles involved. At the end of Appendix A it was checked explicitly that the equations give rise to purely dissipative processes, where dissipation is halted only at equilibrium configurations of coplanarity, circularity and corotation. In the subsequent sections it was assumed that one of the two stars, the companion, had a negligible moment of inertia.

Around the stable equilibrium configurations the tidal evolution equations were linearized and solved in Sect. 3 for two sets of variables. Time scales for the rate of change of the semimajor axis and eccentricity of the orbit and the rotational velocity and inclination of the primary star were derived and discussed. It turns out that an important classification parameter is the ratio α of orbital angular momentum to rotational angular momentum at equilibrium, defined in Eq. (22). Before equilibrium is reached, α

Table 1

α range	Number of areas where							
	$\frac{da}{dt'}<0$	$\frac{da}{dt'}>0$	$\frac{de}{dt'}<0$	$\frac{de}{dt'}>0$	$\frac{d\Omega}{dt'}<0$	$\frac{d\Omega}{dt'}>0$	$\frac{di}{dt'}<0$	$\frac{di}{dt'}>0$
$3<\alpha<10.932$	1	1	1	0	1	1	1	0
$10.932<\alpha<21.532$	1	1	1	1	1	1	1	0
$21.532<\alpha<27.062$	1	1	1	1	1	1	1	1
$27.062<\alpha<35.447$	1	1	1	1	1	2	1	1
$\alpha>35.447$	2	1	2	1	1	2	1	1

$$\frac{di}{dt'}>0 \Rightarrow \frac{de}{dt'}>0 \Rightarrow \frac{da}{dt'}>0 \Rightarrow \frac{d\Omega}{dt'}<0$$

$$\frac{d\Omega}{dt'}>0 \Rightarrow \frac{da}{dt'}<0 \Rightarrow \frac{de}{dt'}<0 \Rightarrow \frac{di}{dt'}<0$$

can be predicted simply from the total amount of angular momentum of the binary system, which is conserved, through Eq. (57).

For cases where the rotational angular momentum is appreciable at equilibrium, i.e. $5 \lesssim \alpha \lesssim 10$, the different time scales are of roughly the same order of magnitude (see Fig. 4). For values of α close to instability, i.e. $3<\alpha \lesssim 5$, the time scales for inclination and eccentricity are much shorter than the other two. But if the rotational angular momentum is relatively small at equilibrium, i.e. $\alpha \gtrsim 10$, the time scale for decrease in eccentricity is far larger than the other three, which are of comparable magnitude. As an effect of this the binary system tends to a state of pseudo-synchronization relatively quickly, which is defined as synchronization of orbital and rotational motion around periastron. The inclination too vanishes on roughly the same short time scale. Only the eccentricity diminishes on a much longer time scale. During this time the changes in semimajor axis and rotational velocity are driven by the slow change in eccentricity, as can be seen clearly in the solutions (36)–(39) to the linearized Eq. (34).

For large deviations from corotation and circularity, many interesting aspects of tidal evolution were found analytically in Sect. 4, with details in Appendix C, as summarized in Table 1. It turns out that again tidal evolution behaviour can be classified according to the value of α. An impression of the general pattern of changes in semimajor axis and eccentricity can be formed from a few numerical solutions depicted in Figs. 5–8 for different values of α. Both the local and global features which were derived analytically can be recognized in these figures.

One of the most interesting aspects of the global behaviour for $\alpha \gtrsim 10$ is the occurrence of turning points in the evolution of both the eccentricity and the semimajor axis, as is clearly visible in Fig. 7. In Sect. 4 this behaviour is discussed, and conditions for its occurrence are mentioned ($\alpha>10.932$). Another result is the uniform decrease of inclination for high eccentricity ($e>\frac{4}{9}\sqrt[4]{17}\simeq 0.9025$), independent of the values of α and the semimajor axis. The same holds true for any eccentricity and semimajor axis if $\alpha<21.532$.

We can conclude that there are a number of interesting relations which can be obtained analytically from the equations for tidal evolution in the weak friction model where the tides have a constant time lag in a corotating coordinate frame. Although the equations are rather cumbersome, including several finite power series in e^2, several relevant combinations of these series still show a simple monotonic behaviour. This surprising result enabled us to obtain many global conclusions, including a general classification of tidal evolution with respect to α.

The model used throughout in the present analysis in admittedly simple, but at the same time it is sufficiently general to be applicable to a wide class of binary stars, at least in a qualitative way. To obtain more realistic models for tidal evolution in close detached binary systems, a detailed study of the relevant physical processes of energy dissipation through tidal interaction is needed. This will certainly give more complicated equations for the tidal evolution of orbit and rotation, with a strong dependence on the particular type of system under study. Nevertheless it is expected that the conclusions derived in this paper will still hold at least qualitatively for a wide range of binary systems. As long as stellar oscillations, giving rise to dynamical tides, do not dominate the tidal evolution the time scales, derived in Sect. 3, and the global classification made in Sect. 4 provide a rather complete general picture of tidal evolution.

Appendix A

From the perturbation of the gravitational force between the two stars, caused by tidal distortion of the primary, equations will be derived for the rate of change of a, e, and Ω: the semimajor axis and eccentricity of the orbit, and the rotational angular velocity of the primary, respectively.

First the effect of the radial perturbation of the gravitational force, given by (8) as

$$F_r = -3G\frac{m^2}{r^2}\left(\frac{R}{r}\right)^5 k\left(1+3\frac{\dot{r}}{r}\tau\right) \tag{A1}$$

will be investigated. Since this is a central force, no angular momentum is exchanged. Therefore both Ω and the orbital angular momentum h remain constant, where h can be expressed in terms of a and e as

$$h^2 = G\frac{M^2m^2}{M+m}a(1-e^2). \tag{A2}$$

The only effect is a dissipation of energy, decreasing the orbital energy

$$E_{\rm orb} = -G\frac{Mm}{2a}. \tag{A3}$$

Thus from $\dot{E}_{\rm orb}$ both $\dot{a}$ and $\dot{e}$ can be derived, using (A2) and (A3) together with $\dot{h}=0$.

The loss of energy over one orbit is

$$\Delta E=\int_{\rm orbit} F_r dr=\int_0^{2\pi} F_r\frac{dr}{d\theta}d\theta, \tag{A4}$$

where θ is the mean anomaly.

Using

$$r=a\frac{1-e^2}{1+e\cos\theta} \tag{A5}$$

we find

$$\Delta E=\int_0^{2\pi} F_r a\frac{e(1-e^2)}{(1+e\cos\theta)^2}\sin\theta d\theta. \tag{A6}$$

The first term of F_r, Eq. (A1), gives no contribution, while the second one gives

$$\Delta E=-9Gm^2R^5k\tau ae(1-e^2)\int_0^{2\pi}\frac{\dot{r}}{r^8}\frac{\sin\theta}{(1+e\cos\theta)^2}d\theta. \tag{A7}$$

Using

$$h=\frac{Mm}{M+m}r^2\dot{\theta} \tag{A8}$$

and (A2) and (A5) we find

$$\dot{r}=\frac{e\sin\theta}{1+e\cos\theta}r\dot{\theta}=\frac{e\sin\theta}{1+e\cos\theta}\frac{M+m}{Mm}\frac{h}{r}$$
$$=G^{1/2}(M+m)^{1/2}a^{-1/2}(1-e^2)^{-1/2}e\sin\theta. \tag{A9}$$

After substitution of (A5) and (A9) in (A7), the integration over θ can be carried out, and results in

$$\Delta E=-9\pi G^{3/2}(M+m)^{1/2}m^2R^5k\tau$$
$$\cdot a^{-15/2}(1-e^2)^{-15/2}e^2\{1+\tfrac{15}{4}e^2+\tfrac{15}{8}e^4+\tfrac{5}{64}e^6\}. \tag{A10}$$

The energy change is negative definite, as it must be for pure dissipation.

To derive the average rate of energy loss, we have to divide this expression by the orbital period, which by Kepler's third law is

$$P=2\pi G^{-1/2}(M+m)^{-1/2}a^{3/2}, \tag{A11}$$

so that

$$\dot{E}_{\rm orb}=-\tfrac{9}{2}G^2(M+m)m^2R^5k\tau a^{-9}(1-e^2)^{-15/2}$$
$$\cdot e^2\{1+\tfrac{15}{4}e^2+\tfrac{15}{8}e^4+\tfrac{5}{64}e^6\}. \tag{A12}$$

This expression can be simplified by defining a typical tidal time scale

$$T=\frac{1}{4\pi^2}\left(\frac{P_s}{\tau}\right)P_s=\frac{R^3}{GM\tau}, \tag{A13}$$

where P_s is the period of the orbit of a test particle grazing over the surface of the primary. This is intuitively clear: expressed in units of a typical orbit, the time scale for significant tidal effects on the orbit is the inverse of the lag time τ.

From (A3) and (A12), using (A13) directly follows

$$\dot{a}=-9\frac{k}{T}q(1+q)\left(\frac{R}{a}\right)^8 a(1-e^2)^{-15/2}$$
$$\cdot e^2\left\{1+\frac{15}{2}e^2+\frac{15}{8}e^4+\frac{5}{64}e^6\right\}, \tag{A14}$$

where q is the mass ratio m/M of the two stars.

From (A2) and $\dot{h}=0$ then follows

$$\dot{e}=-\frac{9}{2}\frac{k}{T}q(1+q)\left(\frac{R}{a}\right)^8(1-e)^{-13/2}$$
$$\cdot e\left\{1+\frac{15}{2}e^2+\frac{15}{8}e^4+\frac{5}{64}e^6\right\}. \tag{A15}$$

As a next step, we must investigate the effect of the component F_θ of the tidal perturbation force transverse to the radius vector, given by (8) as

$$F_\theta=3G\frac{m^2}{r^2}\left(\frac{R}{r}\right)^5 k\tau(\Omega-\dot{\theta}). \tag{A16}$$

This perturbation does exchange angular momentum via a torque $N=rF_\theta$, exerted on the secondary by the tides raised on the primary. The rate of change of a and e can be determined again from (A2) and (A3) after calculating $\dot{E}_{\rm orb}$ and $\dot{h}$. Conservation of total angular momentum then gives $\dot{\Omega}$ as well.

The change in orbital energy over one orbit is

$$\delta E=\int_0^{2\pi} N d\theta=3Gm^2R^5k\tau\int_0^{2\pi} r^{-7}(\Omega-\dot{\theta})d\theta \tag{A17}$$

and with (A2), (A5), (A9), and (A13) this can be written as

$$\delta E=3\frac{k}{T}\frac{m^2}{M}R^8a^{-6}(1-e^2)^{-6}$$
$$\cdot\int_0^{2\pi}\{(1+e\cos\theta)^6\Omega-(1-e^2)^{-3/2}(1+e\cos\theta)^8 n\}d\theta, \tag{A18}$$

where $n=G^{1/2}(M+m)^{1/2}a^{-3/2}$ is the mean orbital angular velocity. After the θ integration, and dividing by the orbital period P, we find the rate of change of the orbital energy

$$\dot{E}_{\rm orb}=-3\frac{k}{T}G(M+m)m^2M^{-1}R^8a^{-9}(1-e^2)^{-15/2}$$
$$\cdot\left\{\left(1+14e^2+\frac{105}{4}e^4+\frac{35}{4}e^6+\frac{35}{128}e^8\right)\right.$$
$$\left.-\frac{\Omega}{n}(1-e^2)^{3/2}\left(1+\frac{15}{4}e^2+\frac{45}{8}e^4+\frac{5}{16}e^6\right)\right\}. \tag{A19}$$

For the orbital angular momentum, the change over one orbit is

$$\delta h=\int_{\rm orbit} N dt=\int_0^{2\pi} N\frac{d\theta}{\dot{\theta}}. \tag{A20}$$

Again using (A2), (A5), (A8), and (A9) we get

$$\delta h=-3\frac{k}{T}\frac{m^2}{M}R^8a^{-6}(1-e^2)^{-6}$$
$$\cdot\int_0^{2\pi}\left\{(1+e\cos\theta)^6-(1-e^2)^{3/2}(1+e\cos\theta)^4\frac{\Omega}{n}\right\}d\theta \tag{A21}$$

which after integration and division by P, gives

$$\dot{h}=-3\frac{k}{T}G^{1/2}(M+m)^{1/2}m^2M^{-1}R^8a^{-15/2}(1-e^2)^{-6}$$
$$\cdot\left\{\left(1+\frac{15}{2}e^2+\frac{45}{8}e^4+\frac{5}{16}e^6\right)\right.$$
$$\left.-\frac{\Omega}{n}(1-e^2)^{3/2}\left(1+3e^2+\frac{3}{8}e^4\right)\right\}. \tag{A22}$$

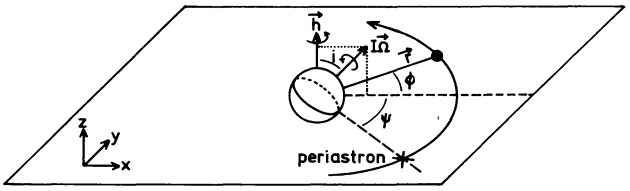

Fig. 10. An illustration of the inclination evolution, as derived in Appendix 2. The orbit lies in the (x, y)-plane, while the line of intersection of the orbital and the equatorial plane coincides with the y-axis

As before, (A3) can be used to convert (A19) to

$$\dot{a}=-6\frac{k}{T}q(1+q)\left(\frac{R}{a}\right)^8 a(1-e^2)^{-15/2}\cdot\left\{\left(1+14e^2+\frac{105}{4}e^4+\frac{35}{4}e^6+\frac{35}{128}e^8\right)-\frac{\Omega}{n}(1-e^2)^{3/2}\left(1+\frac{15}{2}e^2+\frac{45}{8}e^4+\frac{5}{16}e^6\right)\right\}. \tag{A23}$$

To derive the rate of change of e, we can use (A2):

$$\dot{e}=\tfrac{1}{2}(1-e^2)e^{-1}a^{-1}\dot{a}-G^{-1}M^{-2}m^{-2}(M+m)e^{-1}a^{-1}h\dot{h}. \tag{A24}$$

Substituting (A22) and (A23) results in

$$\dot{e}=-\frac{3}{2}\frac{k}{T}q(1+q)\left(\frac{R}{a}\right)^8(1-e^2)^{-13/2}e\cdot\left\{\left(15+\frac{225}{4}e^2+\frac{225}{8}e^4+\frac{75}{64}e^6\right)-\frac{\Omega}{n}(1-e^2)^{3/2}\left(11+\frac{33}{2}e^2+\frac{11}{8}e^4\right)\right\}. \tag{A25}$$

The rate of change of Ω follows from (A22):

$$-\dot{h}=\frac{d}{dt}(I\Omega)=MR^2r_g^2\dot{\Omega}. \tag{A26}$$

Here I is the moment of inertia of the primary and r_g is its radius of gyration ($r_g^2=2/5$ for a homogeneous star, $r_g^2\approx 0.1$–0.01 for a realistic centrally condensed star).

Thus

$$\dot{\Omega}=3\frac{k}{T}\frac{q^2}{r_g^2}\left(\frac{R}{a}\right)^6(1-e^2)^{-6}n\cdot\left\{\left(1+\frac{15}{2}e^2+\frac{45}{8}e^4+\frac{5}{16}e^6\right)-\frac{\Omega}{n}(1-e^2)^{3/2}\left(1+3e^2+\frac{3}{8}e^4\right)\right\}. \tag{A27}$$

To summarize, the equations governing the rate of change $\dot{a}$, $\dot{e}$, and $\dot{\Omega}$ have been determined directly from the perturbing force (8). To obtain $\dot{a}$, (A14) and (A23) are added in (9); and for $\dot{e}$ (A15) and (A24) together form (10). $\dot{\Omega}$ is already given in (A27), which provides (11).

Finally it is interesting to determine the energy dissipation rate, with the total energy given by

$$E=E_{\rm orb}+E_{\rm rot}=-G\frac{Mm}{2a}+\frac{1}{2}MR^2r_g^2\Omega^2. \tag{A28}$$

The first term receives contributions from both the radial (A12) and the transverse (A19) perturbations, together resulting in

$$\dot{E}_{\rm orb}=-3\frac{k}{T}m^2M^{-1}R^8a^{-6}(1-e^2)^{-15/2}\cdot\{(1+\tfrac{31}{2}e^2+\tfrac{255}{8}e^4+\tfrac{185}{16}e^6+\tfrac{25}{64}e^8)n^2-\Omega n(1-e^2)^{3/2}(1+\tfrac{15}{2}e^2+\tfrac{45}{8}e^4+\tfrac{5}{16}e^6)\}, \tag{A29}$$

where Kepler's third law has been used.

The second terms follows directly from (A27):

$$\dot{E}_{\rm rot}=3\frac{k}{T}m^2M^{-1}R^8a^{-6}(1-e^2)^{-6}\cdot\{(1+\tfrac{15}{2}e^2+\tfrac{45}{8}e^4+\tfrac{5}{16}e^6)\Omega n-\Omega^2(1-e^2)^{3/2}(1+3e^2+\tfrac{3}{8}e^4)\}. \tag{A30}$$

For $\Omega\gg n$, energy is transferred from spin to orbit, and for $\Omega\ll n$ from orbit to spin. The same is true for angular momentum, as can be seen from (A22). However, the total energy always decreases as long as $e>0$ or $\Omega\neq n$, as follows from (A29) and (A30):

$$\dot{E}=-3\frac{k}{T}m^2M^{-1}R^8a^{-6}(1-e^2)^{-15/2}n^2\{A-2Bx+Cx^2\}, \tag{A31}$$

where

$$x=\frac{\Omega}{n}(1-e^2)^{3/2}, \tag{A32}$$

$$A=1+\tfrac{31}{2}e^2+\tfrac{255}{8}e^4+\tfrac{185}{16}e^6+\tfrac{25}{64}e^8, \tag{A33}$$

$$B=1+\tfrac{15}{2}e^2+\tfrac{45}{8}e^4+\tfrac{5}{16}e^6, \tag{A34}$$

$$C=1+3e^2+\tfrac{3}{8}e^4. \tag{A35}$$

The energy-loss rate (A31) is minimized, at fixed eccentricity, by $x=B/C$. The expression $\{A-2Bx+Cx^2\}$ in (A31) then becomes D/C, where C is given above, and

$$D=AC-B^2=\tfrac{7}{2}e^2+\tfrac{45}{4}e^4+28e^6+\tfrac{685}{64}e^8+\tfrac{255}{128}e^{10}+\tfrac{25}{512}e^{12}. \tag{A36}$$

Thus only at zero eccentricity can there be zero tidal energy loss, which occurs for $x=1$, i.e. for $\Omega=n$. Tidal dissipation continues until both circularity and corotation are reached.

Appendix B

When the orbital plane does not coincide with the equatorial plane of the primary, the inclination angle between the two planes will change under tidal interaction. To derive the rate of change in the weak friction model where the tides have a constant time lag τ, we will derive the torque exerted on the primary in a frame comoving with the rotation of the primary. In this frame the tidal misalignment is the simplest: the tides point to that position on the celestial sphere where the secondary was situated a time τ before.

Let us start with a simpler non-rotating frame S (Fig. 10) centered on the primary in which the orbit lies in the (x, y)-plane, so that the orbital angular momentum $\boldsymbol{h}$ points in the z-direction:

$$\boldsymbol{h}=h(0,0,1). \tag{B1}$$

The x-axis is chosen so that the rotational angular momentum $I\boldsymbol{\Omega}$ lies in the (x, z) plane:

$$\boldsymbol{\Omega}=\Omega(\sin\tilde{i},0,\cos\tilde{i}). \tag{B2}$$

The position of the secondary is then given by

$$\boldsymbol{r}=a\frac{1-e^2}{1+e\cos(\phi-\psi)}(\cos\phi,\sin\phi,0), \tag{B3}$$

where ψ is the angle from the x-axis to the periastron (ψ is negative in Fig. 10), and ϕ is the angle from the x-axis to the secondary.

Now let us change to a frame S' which is also non-rotating, but where the z'-axis lies along $\boldsymbol{\Omega}$. Denoting components in S' with square brackets, we have

$$\boldsymbol{h}=h[-\sin\tilde{i},0,\cos\tilde{i}], \tag{B4}$$

$$\boldsymbol{\Omega}=\Omega[0,0,1], \tag{B5}$$

$$\boldsymbol{r}=a\frac{1-e^2}{1+e\cos(\phi-\psi)}[\cos\tilde{i}\cos\phi,\sin\phi,\sin\tilde{i}\cos\phi]. \tag{B6}$$

Finally a time dependent transformation brings us to a third frame S'', corotating with the primary, via a rotation in the (x',y')-plane with angular velocity Ω. Using curly brackets for components in S'', we have

$$\boldsymbol{h}=h\{-\sin\tilde{i}\cos\Omega t,\sin\tilde{i}\sin\Omega t,\cos\tilde{i}\}, \tag{B7}$$

$$\boldsymbol{\Omega}=\Omega\{0,0,1\}, \tag{B8}$$

$$\begin{aligned}\boldsymbol{r}=a\frac{1-e^2}{1+e\cos\theta}\{&\cos\tilde{i}\cos(\theta+\psi)\cos\Omega t+\sin(\theta+\psi)\sin\Omega t,\\&-\cos\tilde{i}\cos(\theta+\psi)\sin\Omega t+\sin(\theta+\psi)\cos\Omega t,\sin\tilde{i}\cos(\theta+\psi)\},\end{aligned} \tag{B9}$$

where θ is the mean anomaly, $\theta=\phi-\psi$.

The torque $\boldsymbol{N}$ on the tidal bulge of the primary is the generalization of $-rF_\theta$, where F_θ is the transverse force given in (A17), for finite inclination: In the frame S'' it has the simple form

$$\boldsymbol{N}=3k\tau Gm^2R^5r^{-6}\hat{\boldsymbol{r}}\times\frac{d\hat{\boldsymbol{r}}}{dt} \tag{B10}$$

where

$$\hat{\boldsymbol{r}}=r^{-1}\boldsymbol{r}.$$

Writing out the last factor, we have

$$\begin{aligned}N=3k\tau Gm^2R^5r^{-6}\hat{\boldsymbol{r}}&\\\times[\{&-\cos\tilde{i}\cos(\theta+\psi)\sin\Omega t+\sin(\theta+\psi)\cos\Omega t,\\&-\cos\tilde{i}\cos(\theta+\psi)\cos\Omega t-\sin(\theta+\psi)\sin\Omega t,0\}\Omega\\&+\{-\cos\tilde{i}\sin(\theta+\psi)\cos\Omega t+\cos(\theta+\psi)\sin\Omega t,\\&\cos\tilde{i}\sin(\theta+\psi)\sin\Omega t+\cos(\theta+\psi)\cos\Omega t,\\&-\sin\tilde{i}\sin(\theta+\psi)\}\dot{\theta}].\end{aligned} \tag{B11}$$

Now we can go back to the nonrotating frame S':

$$\begin{aligned}N=3\frac{k}{T}m^2M^{-1}R^8r^{-6}\hat{\boldsymbol{r}}\times[[&\sin(\theta+\psi),-\cos\tilde{i}\cos(\theta+\psi),0]\Omega\\&+[-\cos\tilde{i}\sin(\theta+\psi),\cos(\theta+\psi),-\sin\tilde{i}\sin(\theta+\psi)]\dot{\theta}]\end{aligned} \tag{B12}$$

and to the original frame S:

$$\begin{aligned}N=3\frac{k}{T}m^2M^{-1}R^8r^{-6}\hat{\boldsymbol{r}}\times[&(\cos\tilde{i}\sin(\theta+\psi),-\cos\tilde{i}\cos(\theta+\psi),\\&-\sin\tilde{i}\sin(\theta+\psi))\Omega+(-\sin(\theta+\psi),\cos(\theta+\psi),0)\dot{\theta}].\end{aligned} \tag{B13}$$

Using (B3) this is

$$\begin{aligned}\boldsymbol{N}=3\frac{k}{T}m^2M^{-1}R^8r^{-6}[&(-\sin\tilde{i}\sin^2(\theta+\psi),\\&\sin\tilde{i}\sin(\theta+\psi)\cos(\theta+\psi),-\cos\tilde{i})\Omega+(0,0,1)\dot{\theta}].\end{aligned} \tag{B14}$$

As a next step, we can average over the angle ψ, the angle between periastron and the projection of $\boldsymbol{\Omega}$ on the orbital plane. The reason is that both precession and apsidal motion cause a rotation of ψ on a time scale much shorter than typical tidal time scales; see e.g. Alexander (1973). Averaging over ψ gives the average torque

$$\boldsymbol{N}=3\frac{k}{T}m^2M^{-1}R^8r^{-6}\left[\left(-\frac{1}{2}\sin\tilde{i},0,-\cos\tilde{i}\right)\Omega+(0,0,1)\dot{\theta}\right]. \tag{B15}$$

This torque changes $\boldsymbol{\Omega}$, which can be written with (B2) as

$$\boldsymbol{N}=I\dot{\boldsymbol{\Omega}}=I(\sin\tilde{i},0,\cos\tilde{i})\dot{\Omega}+I\Omega(\cos\tilde{i},0,-\sin\tilde{i})\frac{d\tilde{i}}{dt}. \tag{B16}$$

Equating (B15) and (B16) gives

$$\dot{\Omega}=\frac{3}{I}\frac{k}{T}m^2M^{-1}R^8r^{-6}\left(\dot{\theta}\cos\tilde{i}-\Omega\left(1-\frac{1}{2}\sin^2\tilde{i}\right)\right), \tag{B17}$$

$$\frac{d\tilde{i}}{dt}=\frac{3}{I\Omega}\frac{k}{T}m^2M^{-1}R^8r^{-6}\left(-\dot{\theta}\sin\tilde{i}+\frac{\Omega}{4}\sin2\tilde{i}\right). \tag{B18}$$

However, this result covers only the change in inclination resulting from the change in $\boldsymbol{\Omega}$. By conservation of total angular momentum, $\boldsymbol{h}$ must change as well:

$$\dot{\boldsymbol{h}}=-I\dot{\boldsymbol{\Omega}},$$

giving a second contribution to the change in the inclination.

To simplify the discussion, only terms to first order in $\tilde{i}$ will be retained. A generalization to higher orders in $\tilde{i}$ is straightforward. Since $\dot{\boldsymbol{h}}=-I\dot{\boldsymbol{\Omega}}$ we can parametrize $\boldsymbol{h}$ as

$$\boldsymbol{h}=h(\sin j,0,\cos j) \tag{B19}$$

with $j=0$ initially to reduce to (B1).

In analogy with (B16) we have

$$\dot{\boldsymbol{h}}=(\sin j,0,\cos j)\dot{h}+h(\cos j,0,-\sin j)\frac{dj}{dt}=\left(h\frac{dj}{dt},0,\dot{h}\right). \tag{B20}$$

Angular momentum conservation, $\dot{\boldsymbol{h}}=-\boldsymbol{N}$, gives with (B15)

$$\frac{dj}{dt}=\frac{3}{2}\frac{k}{T}m^2M^{-1}R^8r^{-6}\frac{\Omega}{h}\sin\tilde{i}. \tag{B21}$$

To derive the rate of change of the inclination i, defined as the angle between $\boldsymbol{h}$ and $I\boldsymbol{\Omega}$, to first order in $\tilde{i}$, we subtract (B18) and (B19) after linearization:

$$\frac{di}{dt}=\frac{d}{dt}(\tilde{i}-j)=-3\frac{k}{T}m^2M^{-1}R^8r^{-6}\frac{i}{I\Omega}\left\{\dot{\theta}-\left(1-\frac{I\Omega}{h}\right)\frac{\Omega}{2}\right\}. \tag{B22}$$

Comparing this with the linearized version of (B17)

$$\dot{\Omega}=\frac{3}{I}\frac{k}{T}m^2M^{-1}R^8r^{-6}\{\dot{\theta}-\Omega\}, \tag{B23}$$

we can use (A28) to directly obtain the average over an orbit as

$$\begin{aligned}\frac{d}{dt}i=-3\frac{k}{T}\frac{q^2}{r_g^2}\left(\frac{R}{a}\right)^6(1-e^2)^{-6}\frac{n}{\Omega}i\Big\{&\left(1+\frac{15}{2}e^2+\frac{45}{8}e^4+\frac{5}{16}e^6\right)\\&-\frac{1}{2}(1-\eta)\frac{\Omega}{n}(1-e^2)^{3/2}\left(1+3e^2+\frac{3}{8}e^4\right)\Big\},\end{aligned} \tag{B24}$$

where $i=\tilde{i}-j$ is the inclination, and

$$\eta=\frac{I\Omega}{h}=r_g^2\frac{M+m}{m}\left(\frac{R}{a}\right)^2(1-e^2)^{-1/2}\frac{\Omega}{n} \tag{B25}$$

is the ratio of the rotational and the orbital angular momentum.

Appendix C

Here a derivation will be given of the global features of tidal evolution as summarized in Sect. 4. We will concentrate on the behaviour of the inclination i, which is the most complicated. The changes in $\tilde{a}$, e, and Ω can be analysed in an analogous way.

Equation (13) gives the rate of change of the inclination, restricted to the case of small inclination in which we are interested:

$$\frac{di}{dt}=-3\frac{k}{T}\frac{q^2}{r_g^2}\left(\frac{R}{a}\right)^6(1-e^2)^{-6}\frac{n}{\Omega}i \cdot\left\{f_2(e^2)-\frac{1}{2}(1-\eta)\frac{\Omega}{n}(1-e^2)^{3/2}f_5(e^2)\right\}. \tag{C1}$$

Here η is the ratio of the rotational and orbital angular momentum ($\eta=\alpha^{-1}$ at equilibrium):

$$\eta=r_g^2\frac{M+m}{m}\left(\frac{R}{a}\right)^2(1-e^2)^{-1/2}\frac{\Omega}{n}, \tag{C2}$$

and $f_2(e^2)$ and $f_5(e^2)$ are given by

$$f_2(e^2)=1+\tfrac{15}{2}e^2+\tfrac{45}{8}e^4+\tfrac{5}{16}e^6, \tag{C3}$$

$$f_5(e^2)=1+3e^2+\tfrac{3}{8}e^4. \tag{C4}$$

To analyse the behaviour of the inclination in the $(\tilde{a},e)$-plane we can use Eq. (59), which reads

$$\frac{\Omega}{n}=(1+\alpha)\tilde{a}^{3/2}-\alpha\tilde{a}^2(1-e^2)^{1/2}. \tag{C5}$$

Whether the inclination increases or decreases, depends solely on the sign of the expression between brackets in (C1). If we keep the eccentricity fixed, this expression becomes a function of only one variable $\tilde{a}$, with two fixed parameters e and α.

$$F(\tilde{a};e,\alpha)=f_2(e^2)-\frac{1}{2}(1-\eta)\frac{\Omega}{n}(1-e^2)^{3/2}f_5(e^2). \tag{C6}$$

Substituting (C2) and (C5) in (C6), we find

$$F(\tilde{a};e,\alpha)=f_2(e^2)-f_5(e^2)\left[-\frac{(1+\alpha)^2}{2\alpha}(1-e^2)\tilde{a} +\frac{3}{2}(1+\alpha)(1-e^2)^{3/2}\tilde{a}^{3/2}-\alpha(1-e^2)^2\tilde{a}^2\right]. \tag{C7}$$

For very small or very large $\tilde{a}$ values $F(\tilde{a};e,\alpha)$ is always positive, which means that the inclination always decreases for very large or very small $\tilde{a}$, independent of e and α:

$$F(0;e,\alpha)=f_2(e^2)>1; \tag{C8}$$

$$\lim_{\tilde{a}\to\infty}\tilde{a}^{-2}F(\tilde{a};e,\alpha)=\alpha(1-e^2)^2f_5(e^2)>0. \tag{C9}$$

To analyse the behaviour for intermediate $\tilde{a}$, we take the derivative

$$F'(\tilde{a};e,\alpha)=(1-e^2)f_5(e^2) \cdot\left[\frac{(1+\alpha)}{2\alpha}-\frac{9}{4}(1+\alpha)(1-e^2)^{1/2}\tilde{a}^{1/2}+2\alpha(1-e^2)\tilde{a}\right], \tag{C10}$$

which has only one positive root

$$\tilde{a}_0=\left[\frac{9}{16}\frac{1+\alpha}{\alpha}\left\{1+\frac{\sqrt{17}}{9}(1-e^2)^{-1/2}\right\}\right]^2. \tag{C11}$$

Furthermore $F''(\tilde{a}_0;e,\alpha)>0$, independent from the values of e and α. Thus $F(\tilde{a};e,\alpha)$ attains its only minimum for positive $\tilde{a}$ at $\tilde{a}_0$.

Substituting (C11) in (C7), the minimum $F(\tilde{a}_0;e,\alpha)$ can be determined. It turns out that the two parameters e and α are surprisingly well separated, which will make the following analysis much simpler:

$$\min_{0<\tilde{a}<\infty}F(\tilde{a};e,\alpha)=F(\tilde{a}_0;e,\alpha)=f_2(e^2)-f_5(e^2)k(e^2)\frac{(1+\alpha)^4}{\alpha^3}, \tag{C12}$$

where

$$k(e^2)=-\tfrac{1}{2}h^2(e^2)+\tfrac{3}{2}h^3(e^2)-h^4(e^2). \tag{C13}$$

and

$$h(e^2)=\tfrac{1}{16}\{\sqrt{17}+9(1-e^2)^{1/2}\}. \tag{C14}$$

Thus we can conclude that for fixed α and e the inclination will increase for one connected range of $\tilde{a}$ values, if and only if $F(\tilde{a}_0;e,\alpha)<0$, or with (C12):

$$P(e)=\frac{f_2(e^2)}{f_5(e^2)k(e^2)}<\frac{(1+\alpha)^4}{\alpha^3}=Q(\alpha). \tag{C15}$$

If $P(e)>Q(\alpha)$, then the inclination decreases for all $\tilde{a}$ values. In the critical case where $P(e)=Q(\alpha)$, there is only one point where the inclination is stationary; for all other $\tilde{a}$ values it decreases. However, these conclusions are valid only for $0\leqq e\lesssim 0.9025$ where $P(e)>0$. For higher eccentricity $P(e)$ changes sign, and $F(\tilde{a}_0;e,\alpha)>0$ independent of α. Thus for all eccentricity above a critical value $e_{cr}\simeq 0.9025$ the inclination always decreases, independent of $\tilde{a}$ and α.

The two functions $P(e)$ en $Q(\alpha)$ are plotted in Fig. 11. It can be seen that $Q(\alpha)$ and $P(e)$ are both monotonously increasing, at least for $e<e_{cr}$. At e_{cr}, $P(e)$ jumps from $+\infty$ to $-\infty$, since $k(e^2)$ in Eq. (C13) goes through zero. With (C13) and (C14) then follows $e_{cr}=\frac{4}{9}\sqrt[4]{17}\simeq 0.9025$. For a given value of α, the maximum eccentricity $e_{\max}$ for which the inclination can be stationary can be determined from Fig. 11 by equating $P(e_{\max})=Q(\alpha)$. The monotonous increase of $P(e)$ then guarantees the existence of two stationary points in the $(\tilde{a},e)$-plane for all values $e<e_{\max}$.

The critical α value below of which the inclination decreases everywhere is obtained when $e_{\max}=0$. From (C13) and (C15) we thus obtain a quartic equation for α_{cr}:

$$\frac{(1+\alpha_{cr})^4}{\alpha_{cr}^3}=\frac{1}{k(0)}=\frac{8192}{107+51\sqrt{17}}, \tag{C16}$$

which gives

$$\alpha_{cr}\simeq 21.5322.$$

Finally we will show that an increasing inclination implies an increasing eccentricity as well. We have seen above that the area of increasing inclination is simply connected in the $\{\tilde{a},e\}$-plane. The same can be derived for the area of increasing eccentricity. Thus it is sufficient to prove that stationary eccentricity $\left(\frac{de}{dt}=0\right)$ always implies decreasing inclination $\left(\frac{di}{dt}<0\right)$. This then implies that the area of increasing inclination is contained inside the area of

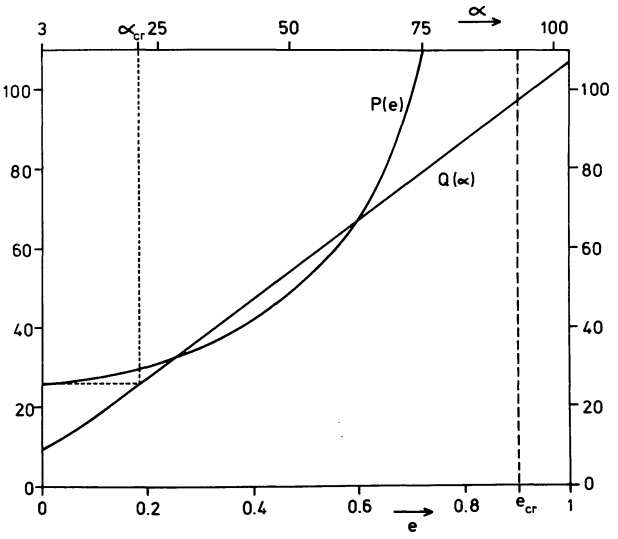

Fig. 11. The auxiliary functions $P(e)$ and $Q(\alpha)$, which are useful for investigating the behaviour of the inclination as derived in Appendix C

increasing eccentricity if they have at least one point in common. It is obvious from Fig. 9 that this is the case for $\alpha=25$. By continuity this holds also for all other values of $\alpha>3$, if the curves of stationary e and i never cross, i.e. if $\frac{de}{dt}=0$ implies $\frac{di}{dt}<0$ strictly for all α.

To prove this, starting with $\frac{de}{dt}=0$, Eq. (10) gives

$$\frac{\Omega}{n}=\frac{18}{11}\frac{f_3(e^2)}{f_4(e^2)}(1-e^2)^{-3/2}, \tag{C17}$$

where

$$f_3(e^2)=1+\tfrac{15}{4}e^2+\tfrac{15}{8}e^4+\tfrac{5}{64}e^6; \tag{C18}$$

$$f_4(e^2)=1+\tfrac{3}{2}e^2+\tfrac{1}{8}e^4. \tag{C19}$$

Substituting (C17) in (C1), the equation for i reads

$$\frac{di}{dt}=-\frac{11}{6}\frac{k}{T}\frac{q^2}{r_g^2}\left(\frac{R}{a}\right)^6(1-e^2)^{-9/2}\frac{f_4(e^2)}{f_3(e^2)}i \cdot\left\{f_2(e^2)-\frac{9}{11}\frac{f_3(e^2)}{f_4(e^2)}f_5(e^2)(1-\eta)\right\}. \tag{C20}$$

Here we have the anticipated result: the expression between brackets is positive for all $\eta>0$, since the function

$$R(e)=\frac{11}{9}\frac{f_2(e^2)f_4(e^2)}{f_3(e^2)f_5(e^2)} \tag{C21}$$

is larger than unity for any eccentricity. In fact, $R(e)$ is a monotonically increasing function, with

$$\tfrac{11}{9}=R(0)\leqq R(e)\leqq R(1)=\tfrac{616}{195} \tag{C22}$$

Thus we have proven that $\frac{de}{dt}=0$ implies $\frac{di}{dt}<0$. As discussed above, this again implies

$$\frac{di}{dt}>0\rightarrow\frac{de}{dt}>0, \tag{C23}$$

one of the relations listed in the second half of Table 1.

Acknowledgements. The author would like to thank J. P. de Cuyper, H. Henrichs, E. P. J. van den Heuvel, F. Verbunt, and F. Verhulst for comments on the manuscript.

References

Alexander, M.E.: 1973, *Astrophys. Space Sci.* **23**, 459
Brouwer, D., Clemence, G.M.: 1961, Celestical Mechanics, Academic Press, New York, London
Counselman, C.C.: 1973, *Astrophys. J.* **180**, 307
Darwin, G.H.: 1879, *Phil. Trans. Roy. Soc.* **170**, 1
Hut, P.: 1980, *Astron. Astrophys.* **92**, 167
Kopal, Z.: 1978, Dynamics of close binary systems, Reidel, Dordrecht
Lecar, M., Wheeler, J.C., McKee, C.F.: 1976, *Astrophys. J.* **205**, 556
Mignard, F.: 1979, 1980, *The Moon and the Planets* **20**, 301; **23**, 185
Zahn, J.-P.: 1977, *Astron. Astrophys.* **57**, 383